J. Biophotonics **6**, No. 5, 425–434 (2013) / **DOI** 10.1002/jbio.201200047

Journal of BIOPHOTONICS

FULL ARTICLE

Synergy of photoacoustic and fluorescence flow cytometry of circulating cells with negative and positive contrasts

Dmitry A. Nedosekin[*,1], *Mustafa Sarimollaoglu*[1], *Ekaterina I. Galanzha*[1], *Rupa Sawant*[2], *Vladimir P. Torchilin*[2], *Vladislav V. Verkhusha*[3], *Jie Ma*[4], *Markus H. Frank*[4], *Alexandru S. Biris*[5], *and Vladimir P. Zharov*[1]

[1] Arkansas Nanomedicine Center, Phillips Classic Laser and Nanomedicine Laboratories, University of Arkansas for Medical Sciences, Little Rock, AR 72205, USA
[2] Center for Pharmaceutical Biotechnology and Nanomedicine, Bouve College of Health Sciences, Northeastern University, Boston, MA 02115, USA
[3] Department of Anatomy and Structural Biology and Gruss-Lipper Biophotonics Center, Albert Einstein College of Medicine, Bronx, NY 10461, USA
[4] Transplantation Research Center, Children's Hospital Boston, Harvard Medical School, Boston, MA 02115, USA
[5] Department of Applied Science and Nanotechnology Center, University of Arkansas at Little Rock, Little Rock, AR 72205, USA

Received 16 March 2012, revised 6 July 2012, accepted 17 July 2012
Published online 21 August 2012

Key words: in vivo cytometry, photoacoustics, fluorescence detection, negative contrast, circulating tumor cells, liposomes, nanoparticles, in vitro flow cytometry

In vivo photoacoustic (PA) and fluorescence flow cytometry were previously applied separately using pulsed and continuous wave lasers respectively, and positive contrast detection mode only. This paper introduces a real-time integration of both techniques with positive and negative contrast modes using only pulsed lasers. Various applications of this new tool are summarized, including detection of liposomes loaded with Alexa-660 dye, red blood cells labeled with Indocyanine Green, B16F10 melanoma cells co-expressing melanin and green fluorescent protein (GFP), C8161-GFP melanoma cells targeted by magnetic nanoparticles, MTLn3 adenocarcinoma cells expressing novel near-infrared iRFP protein, and quantum dot-carbon nanotube conjugates. Negative contrast flow cytometry provided label-free detection of low absorbing or weakly fluorescent cells in blood absorption and autofluorescence background, respectively. The use of pulsed laser for time-resolved discrimination of objects with long fluorescence lifetime (e.g., quantum dots) from shorter autofluorescence background (e.g., blood plasma) is also highlighted in this paper. The supplementary nature of PA and fluorescence detection increased the versatility of the integrated method for simultaneous detection of probes and cells having various absorbing and fluorescent properties, and provided verification of PA data using a more established fluorescence based technique.

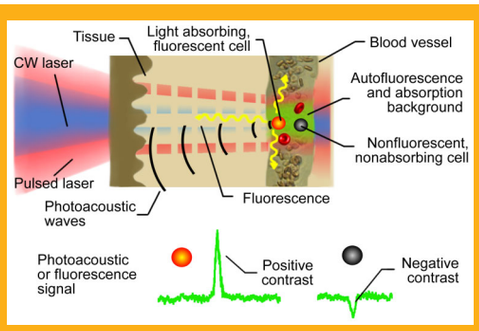

The principles of integrated photoacoustic and fluorescence flow cytometry using positive contrast for detection of strongly absorbing and fluorescent cells and negative contrast for detection of weakly absorbing and fluorescent cells in blood absorption and autofluorescence background, respectively.

* Corresponding author: e-mail: DNedosekin@uams.edu

Journal of
BIOPHOTONICS

1. Introduction

Conventional flow cytometry is a well-established analytical tool that provides quantification of multiple biological parameters of cells at molecular levels, including their functional states, morphology, composition, proliferation, and protein expression [1]. Recent trends in flow cytometry dictated the increase in the number of molecular tags from two to three, to a maximum of 20. In addition, invasive extraction of cells from the blood or lymph circulatory system for magnetic isolation [2, 3] or for conventional flow cytometry analysis may alter cell properties (e.g., morphology or marker expression) and may prevent the long-term study of cells in their native complex biological environment [4, 5]. *Ex vivo* blood analysis is possible only at discrete time points, and dramatically limits the study of rapid changes in circulating objects. Blood collection may also hinder proliferation studies, and cause undesired responses from the immune system, thus, hindering blood cells studies, and may even require sacrificing the animal to assess a large volume of blood.

In vivo flow cytometry is a novel research tool which can provide noninvasive real-time monitoring of: circulating nanoparticles (NPs), normal and abnormal cells (e.g., tumor or bacteria) or drug delivery vehicles (e.g. liposomes) directly within the blood and lymph flow [4]. This tool utilizes various detection platforms including photothermal (PT), fluorescent, photoacoustic (PA), or Raman techniques [4–11]. However, the use of only one technique limits the range of objects to those with either nonradiative or radiative relaxation of the absorbed laser energy. This also restricts the number of tags available for multiplex targeting due to the overlapping of broad absorption or emission spectra. At the current stage, *in vivo* cytometry uses either two fluorescence [4, 5, 12] or PA [13] channels in different spectral ranges.

The number of spectral bands (colors) and the corresponding tags may be increased by the use of ultrasharp nonlinear PT and PA resonances having spectral widths of a few nanometers [14]. Alternatively, multicolor capabilities of *in vivo* flow cytometry may be improved by the use of multimodal schematics in which signals are acquired from different types of contrast agents (e.g., light absorbing and fluorescent tags) and can be detected independently. In 2005, we suggested an integration of PT, PA, fluorescence and scattering methods in *in vivo* flow cytometry [15, 16]. The combination of fluorescence and PA methods has also been demonstrated in microscopy and tomography [17, 18]. However, the integration of PA and fluorescence in *in vivo* cytometry has not been reported yet.

In this paper, we will fill this gap by combining PA flow cytometry (PAFC) and fluorescence flow cytometry (FFC) into a multimodal PA-fluorescence flow cytometry (PAFFC) system with a focus on its novel schematics and modes.

2. Materials and methods

2.1 *In vivo* PA-fluorescence cytometry

The principles of *in vivo* multimodal flow cytometry integrating PA and fluorescence techniques and operating both in positive and in negative contrasts modes [19] are illustrated in Figure 1. In PAFC (Figure 1A), strongly absorbing targets (e.g., gold NPs or red blood cell (RBC) aggregates [red clots]) provide positive PA contrast. Such objects under the laser beam in the vessel produce a transient increase in local absorption, which results in a sharp positive PA peak (Figure 1C) exceeding the level of background signal. Higher absorbance of labeled objects enhances its PA contrast, thus, increasing the chances of detection. The PA background is associated with absorption of randomly distributed RBCs in the irradiated volume. On the contrary, negative PA contrast is produced by a low-absorbing target (e.g.,

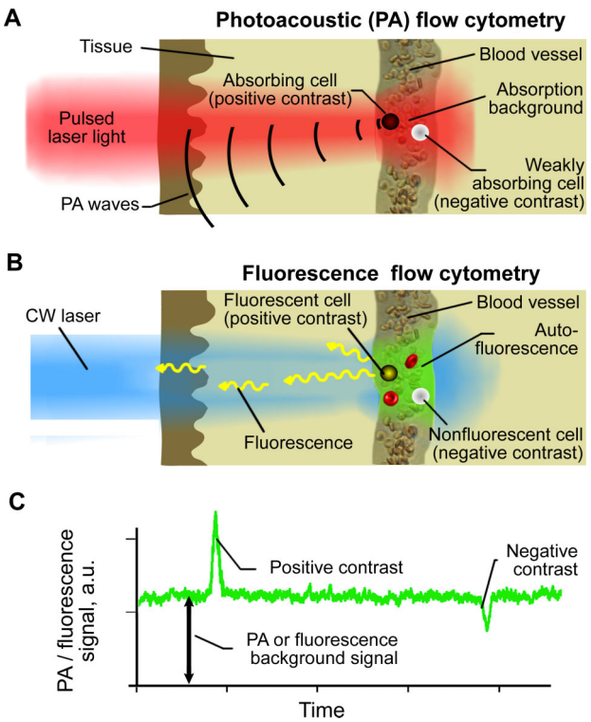

Figure 1 Principles of *in vivo* PAFCC with positive and negative contrasts. (**A**) *In vivo* PA flow cytometry (PAFC). (**B**) *In vivo* fluorescence flow cytometry. (**C**). Example of positive and negative contrast signals.

non-pigmented CTCs, white blood cells (WBCs) or a platelet-rich [white] clot), leading to transient decrease in local absorption and resulting in a sharp negative PA peak (Figure 1C). In our previous studies [19], we proposed that a similar approach can be used in *in vivo* FFC (Figure 1B), when strongly (e.g., labeled cell) and weakly fluorescent objects (e.g., unlabeled RBCs, or fluorescence quenchers) will increase or reduce fluorescence intensity, respectively (Figure 1C). Background fluorescence is associated with auto-fluorescence of blood plasma components, or may be enhanced by intravenous injection of a fluorescence dye (e.g., fluorescein isothiocyanate [FITC]).

Sensitivity of *in vivo* flow cytometry can be expressed as a minimal number of detected abnormal cells in the individual's blood pool and was demonstrated to be as low as 1CTC/mL [13]. Further increases in the sensitivity may be achieved with the analysis of larger blood volumes, as the volume of tested blood is only limited by the experiment duration and blood vessel size.

2.2 Multimodal flow cytometer

The integrated multimodal PAFFC system (Figure 2A) was built on the platform of an Olympus IX81 inverted microscope (Olympus America, Inc., USA), which was equipped with the following high-pulse-repetition-rate lasers: 1) wavelength, 532 nm; maximum pulse energy, 25 μJ; pulse width, 5.3 ns; pulse rate, 10–50 kHz (LUCE 532, Bright Solutions, Italy); 2) 671 nm, 30 μJ, 25 ns, 10–30 kHz (QL671-500, CrystaLaser, Reno, NV); 3) 820 nm, 35 μJ, 8 ns, 10 kHz (LUCE 820, Bright Solutions, Italy); and continuous wave (CW) diode laser with a wavelength of 488 nm and power of 50 mW (IQ1C45(488-60) G26, Power Tech., Alexander, AR). One of the pulsed lasers was either used alone for both PA and FFC systems or it was supplemented by a CW laser for separate generation of PA and fluorescence signals, respectively. Laser beams were focused into the blood vessel by a 40× microobjective (NA 0.65; Olympus), which simultaneously collected fluorescence. Cylindrical lenses ($f = 250$ mm) provided the linear shape of the laser beams in the sample (10 × 80 μm) (Figure 2D).

The simultaneous use of both pulsed and CW laser sources required two dichroic mirrors to separate laser light and fluorescence emission (Figure 2A). A single dichroic mirror was sufficient in PAFFC with the same pulsed laser simultaneously exciting PA and fluorescence from the same object (Figure 2B). The fluorescence was detected by a photomultiplier tube (PMT, R928, Hamamatsu, Co., Bridgewater, NJ) after a bandpass filter having central wavelength

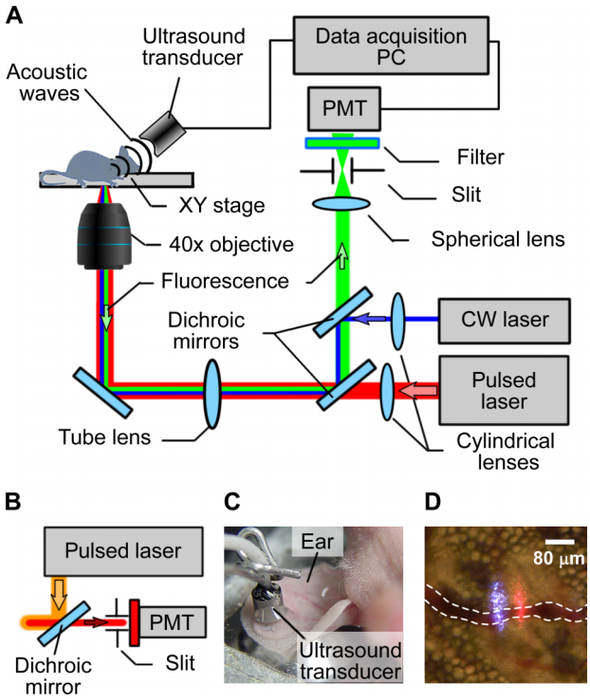

Figure 2 Multimodal cytometry. (**A**) Schematics of the integrated *in vivo* cytometer with pulsed and CW laser sources. Ultrasound transducer and photomultiplier tubes (PMT) detect PA and fluorescence signals, respectively. (**B**) Optical scheme for simultaneous excitation of both PA and fluorescence by the same pulsed laser. (**C**) Ultrasound transducer on a mouse ear. (**D**) An image of two laser beams (488 nm and 671 nm) passed through a blood vessel (dotted line) and ear tissues.

of 520 ± 15 nm for CW 488 nm laser, 580 ± 20 nm for pulsed 532 nm laser; or 720 ± 30 nm for pulsed 671 nm laser (Semrock, Inc., Rochester, NY). A 200 μm × 3 mm slit in the front of the PMT was confocal with the image plane, and provided spatial filtration of the out-of-plane fluorescence. Laser-induced acoustic waves were acquired by an ultrasound transducer (XMS-310, Panametrics NTD Inc., Waltham, MA) directly attached to the skin (Figure 2C), and amplified (50 kHz–5 MHz bandwidth, 54 dB gain, model 5662, Panametrics NDT Inc.). *In vitro* calibration of PAFFC was performed in 96 μm square-shaped quartz capillaries (Polymicro Tech., Phoenix, AZ).

2.3 Data treatment

In the FFC module, signals from the PMT were continuously sampled at 4 MHz rate by a high-speed digitizer (PCI-5124, National Instruments, Austin, TX)

and downsampled to 10 kHz rate with an average of 400 points. In the PAFC module, PA signals from the ultrasound transducer were acquired at a rate of 125 MS/s for 6 μs after each laser pulse and processed by a custom digitizer (AD484; 4DSP Inc., Reno, NV). PA and fluorescence signal traces were displayed on-line and recorded for off-line processing. Trace analysis was made by custom software (LabView, 8.5, National Instruments) and included identification of peaks with the amplitude exceeding the selected threshold, counting the events, and calculating location, amplitude and width for each peak. Bland-Altman statistical analysis was used to compare the results of PA and fluorescence detection. Statistica 5.11 software (StatSoft, Inc., USA) and MATLAB 7.0.1 (MathWorks) were used for the statistical calculations.

2.4 Animal models

In vivo studies were performed using the nude mouse ear model. The animal protocols were approved by the University of Arkansas for Medical Sciences Institutional Animal Care and Use Committee. Animals were anesthetized using Isoflurane (inhalation, 1.1%), and placed on a temperature-controlled stage (37 °C). Cells, NPs, or fluorescent dyes were introduced via intravenous injection into the mouse tail vein. Subcutaneous inoculations of 10^6 C8161 cells expressing green fluorescent protein (GFP) into 50 μL suspension were used to establish primary melanoma xenograft tumors on the backs of the mice.

2.5 Reagents and cells

Fluorescent carboxyl 8.34 μm magnetic particles (FCM-8056-2, Spherotech, Lake Forest, IL) loaded with Red Nail fluorophore (excitation/emission: 480 nm/505 nm) were used simultaneously as both PA and fluorescent contrast agents. Two antibody samples to target melanoma-associated chondroitin sulfate proteoglycan (MCSP), a cell-surface antigen specific for human melanoma [20], were purchased from Miltenyi Biotec Inc. (Auburn, CA) with a conjugation either to magnetic 50 nm NPs or phycoerythrin (PE) fluorescent dye. Dual-contrast quantum dot-carbon nanotube (QD-CNT) conjugates were synthesized as described previously [21]. Alexa-660 modified 250 nm liposomes (2 mol% of Alexa-660-PEG2000-PE, absorption/emission wavelength maxima, 663/690 nm) have been prepared from a mixture of hydrogenated phosphatidylcholine, cholesterol and PEG2000-PE (65 : 30 : 3 mol%) by the lipid film hydration method with subsequent sizing extrusion in Torchilin's laboratory.

The RBCs extracted from the blood of the mice were labeled with Indocyanine Green (ICG) by incubation of 2.5×10^8 RBCs with 85 μg of 0.2 μm-filtered ICG for 60 min at 37 °C followed by washing via centrifugation (1,000 × g for 10 min, twice). Mouse melanoma B16F10 cells were purchased from ATCC (Manassas, VA). Prior to the injection, cells were labeled with fluorescein isothiocyanate (FITC, 0.7 mg/mL, 20 min incubation, 37 °C). The transgenic B16F10-GFP melanoma cell line was created by inserting a pEGFP-N1 vector (Clontech) with Lipofectamine 2000 transfection agent (Invitrogen). Transgenic C8161-GFP human melanoma cells were prepared as described previously [22]. MTLn3 rat adenocarcinoma cells expressed a near-infrared (NIR) bacteriophytochrome-derived fluorescent protein, called iRFP, with absorption/emission maxima at 690/713 nm [23]. All the cells were cultured according to the ATCC recommendations. Fluorescence imaging was used to calculate the percentage of fluorescent cells in the sample. The viability of cells was tested by Trypan Blue staining before injection. Injection of 50 μL of FITC-dextran (Sigma-Aldrich, Inc. St. Louis, MO) was used for enhancing blood plasma autofluorescence.

3. Results

3.1 Multimodal detection of objects with dual photoacoustic-fluorescence contrast

Fluorescent carboxyl 8.34 μm magnetic microbeads were used to calibrate PAFFC *in vitro* in a quartz flow unit. These microbeads were loaded with Nail Red fluorophore and provided dual fluorescence and PA contrast (Figure 3A). Natural absorbance of magnetic material which gradually decreased from visible to the NIR range provided high PA contrast. The influence of the pulsed lasers at 671 nm and 820 nm on fluorescence detection was minimal, while the CW laser did not produce measurable PA signals. Bland-Altman statistical analysis (Figure 3B) of PA and fluorescence signal counts revealed a match for >90% of all beads (Figure 3A). PAFC and FFC modes provided accurate results for counting individual beads at flow velocities ranging from 0.1 to 30 mm/s.

Next, we analyzed the performance of PAFFC *in vivo*. B16F10 melanoma cells (Figure 3C) were detected *in vivo* directly in blood flow after tail vein injection of 10^5 cells. Melanin produced by melanoma cells is an intrinsic PA contrast agent. Contrast for fluorescence detection of nonfluorescent B16F10

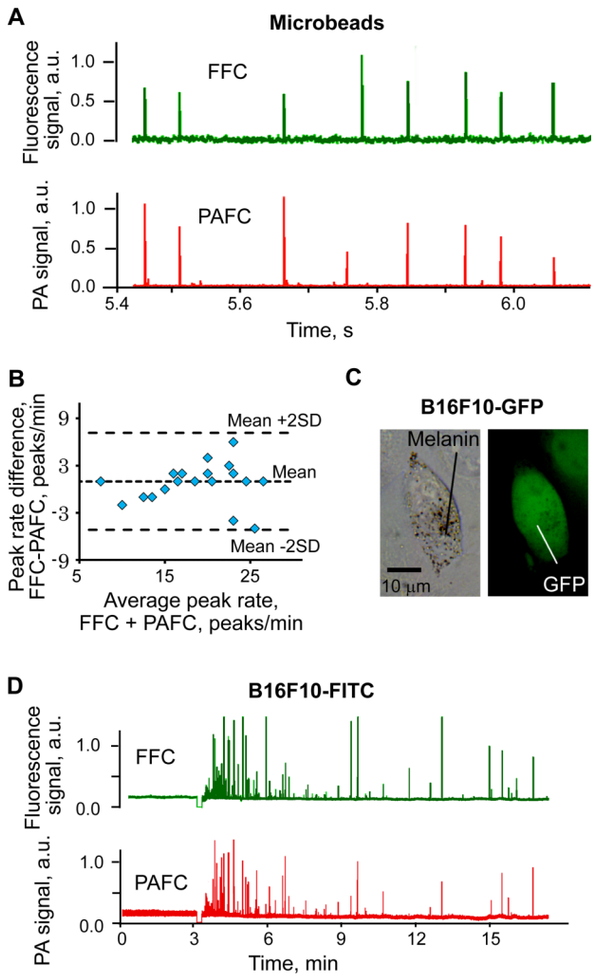

Figure 3 Multimodal PA and fluorescence detection *in vitro* and *in vivo*. (**A**) Detection of fluorescent magnetic microbeads by PAFFC *in vitro* at flow velocity of 10 mm/s. (**B**) Bland-Altman statistics for *in vitro* counting of magnetic microbeads by PA and fluorescence techniques. (**C**) Dual contrast pigmented B16F10-GFP melanoma cells, transmission (left) and fluorescence (right) images. (**D**) *In vivo* detection of FITC labeled B16F10 cells. Wavelength and energy fluence or intensity for PAFC and FFC, respectively: 820 nm, 200 mJ/cm^2 and 488 nm, 80 W/cm^2. Fluorescence imaging exposure: 0.1 s.

cells was provided by labeling cells *in vitro* by FITC with 99.5% efficiency at 96% final cell viability. Significant variation in B16F10 cell's pigmentation (melanin content) ranged from the presence of a few highly pigmented cells to a significant number (15–25%) of cells with weak pigmentation, i.e. with low PA contrast. As a result, the efficiency of label-free PA detection of B16F10 cells was lower than that of fluorescence detection of FITC labeled cells (Figure 3D). Our findings included PA signals which exceeded the detection threshold for about 73 ± 10% (mean ± standard deviation for 3 injections) of the B16F10 cells detected by FFC in the blood vessel, which correlated well with our previous data [24]. Next, we used B16F10 cells expressing GFP. In this case, lower efficacy of both PAFC and FFC was observed. In total, GFP was expressed in 89% of B16F10 cells which was lower than the efficacy of *in vitro* FITC labeling. Many cells expressing high levels of GFP had low pigmentation and vice versa. As a result, PA signal exceeded the detection threshold for 57% of the B16F10-GFP cells detected by *in vivo* fluorescent flow cytometry. Thus, the integrated system provided direct verification of label-free PA detection of melanoma cells through the use of FITC labeling and fluorescent detection of every cell in the blood flow.

3.2 In vivo monitoring of cell – nanoparticle interaction

Next, we used a dual detection to study the interaction between CTCs expressing fluorescent protein and absorbing NPs. Previously, we have reported the tumorigenic potential of melanoma CTCs through the isolation of cells from blood and their characterization *in vitro* [22]. Here, we used PAFFC for *in vivo* characterization of CTCs by targeting them in the blood flow using light-absorbing NPs acting as PA positive contrast agents. To this end, we selected the C8161 melanoma cell line with GFP which provided positive fluorescence contrast. Fifty nm magnetic NPs conjugated to anti-MCSP antibody were used as PA contrast agents and provided molecular-specific interaction with MCSP receptors at the melanoma cell surface. Hence, only those melanoma cells that expressed MCSP to be targeted by these NPs, and non-labeled cells were expected to produce only GFP signals.

MCSP expression of the C8161-GFP cell line was assessed by conventional *in vitro* flow cytometry with fluorescent PE-anti-MCSP antibodies. Fifty-one percent of the C8161-GFP cells expressed MCSP. Accumulation of magnetic NPs in cells during incubation was revealed by PA detection at 820 nm. PA signals for approximately 60% of cells increased 10–20 fold after incubation with NPs, as compared to the level of signals from the non-incubated cells; thus, increasing PA contrast of these cells and the probability of detecting them in blood flow.

In the control mice (i.e., with no tumor) PA detection at 820 nm after the injection of 50 nm magnetic anti-MCSP NPs (10^{11} particles/mL; 10 μL of solution) revealed a few PA signals exceeding the blood background during first 3–5 min after injection. These signals were likely associated with small

Journal of
BIOPHOTONICS

NP clusters rapidly cleared from blood circulation or with the nonspecific binding of these nanoparticles to Fc receptor positive cells [5]. Next, PAFFC was used to monitor the interaction of NPs and CTCs in the blood of a tumor-bearing mouse on Day 20 after subcutaneous inoculation of C8161-GFP cells. FFC with 488 nm CW laser revealed the presence of CTCs in circulation at a rate of ~10 CTCs/h in the 50 μm ear artery (Figure 4, top). After the injection of NPs, we immediately observed several PA signals associated with small NP clusters (Figure 4, bottom), having no matches in the fluorescence trace. PA signals appeared again 30–40 minutes after injection and matched the fluorescent data. In total, 7 fluorescent events were detected by FFC, and for only 3 of those, the amplitude of PA signal exceeded detection threshold.

Thus, both the appearance of signals in time and the matching of PA and fluorescence data can be used to confirm molecular targeting of CTCs by the functionalized anti-MSCP NPs. The majority of false-positive PA signals were associated with NP aggregates rapidly cleared from circulation. The labeling time for the cells was estimated to be approximately 20–40 minutes, as this was the time that the first labeled CTCs appeared in the circulation. Matching of PA and fluorescence signals decreased the probability of detecting false-positive signals due to nonspecific binding [5]. The obtained *in vivo* data matched the MCSP expression levels for the used C8161-GFP cell line. PAFFC provided both the total cell count and enumeration of the cells expressing MCSP. The analogous *ex vivo* study with magnetic extraction of NP-labeled CTCs from blood resulted in counting only MCSP expressing cells [2, 3]. Future studies will focus on analysis of a larger CTC number to confirm our current data on MSCP expression in metastatic melanoma cells.

3.3 *Multimodal photoacoustic-fluorescence cytometry with a pulsed laser source*

We developed an *in vivo* flow cytometer with a simplified scheme using the same pulsed laser for simultaneous generation of both PA and fluorescence signals from the same circulating objects. Specifically, a pulsed laser operating at 532 nm was used to detect circulating QD-CNT conjugates having a relatively large quantum yield associated with QDs and high PA contrast of CNTs [21]. Simultaneous PA and fluorescence signals (Figure 5A) were detected after injection of these NPs, proving the feasibility of *in vivo* PAFFC using pulsed nanosecond lasers. Circulation dynamics data for QD-CNTs demonstrated a clearance rate typical for NPs (Figure 5B). High-speed signal recording (1.0 GHz digitations) revealed that fluorescence signals from QD-CNTs lasted longer (45–70 ns) than the duration of autofluorescence from blood (Figure 5C). This correlated with data from the literature [25] for pure QDs. Thus, time-resolved selection of signals having different fluorescence lifetime may reduce the influence of the autofluorescence background on the detection threshold of QDs, which is difficult to achieve using

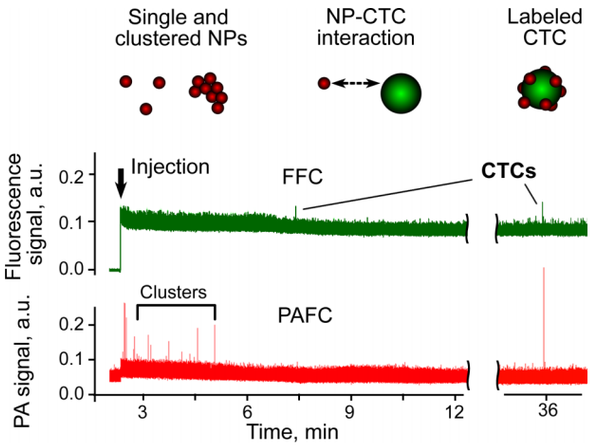

Figure 4 *In vivo* multimodal PA (**red**) and fluorescence (**green**) detection of CTCs (C8161-GFP) in tumor-bearing mouse using functionalized magnetic NPs and GFP as PA and fluorescent contrast agents, respectively. Black arrow marks the moment of NP injection. Wavelength and energy fluence/intensity for PAFC and FFC: 820 nm, 50 mJ/cm^2 and 488 nm, 80 W/cm^2, respectively.

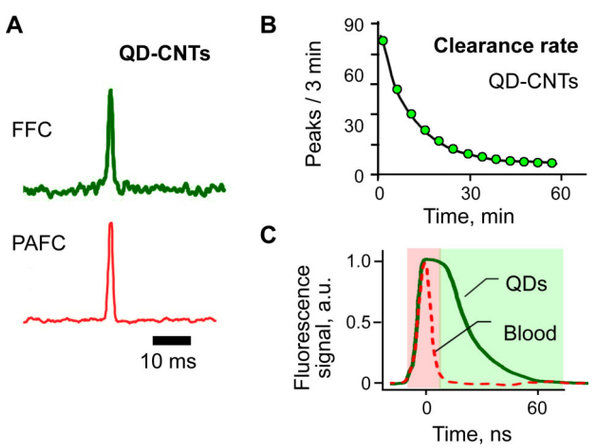

Figure 5 PAFFC with pulsed laser. (**A**) Typical fluorescence (top) and PA (bottom) signals from QD-CNT conjugates in the mouse circulation. (**B**) Clearance rate for QD-CNT conjugates. (**C**) Time-resolved detection of long-lasting fluorescence from QDs in the presence of short-lasting fluorescence from blood. Laser parameters: wavelength, 532 nm; pulse duration, 5 ns; fluence, 50 mJ/cm^2.

traditional CW lasers for the excitation of fluorescence.

We also integrated both PA and fluorescence detection using a pulsed 671 nm laser. The most conventional fluorophores in the NIR tissue transparency window usually are hindered either by their low absorption or low quantum yield. However, low quantum yields of fluorophores are frequently associated with fast, non-radiative relaxation, which increases PA contrast [18]. Thus, integrated PA and fluorescence technique may provide detection of fluorophores having various quantum yields. Specifically, PAFFC with pulsed 671 nm excitation demonstrated successful PA and fluorescence monitoring of intravenously injected liposomes loaded with Alexa660 dye, RBCs labeled with ICG, and MTLn3-iRFP adenocarcinoma cells.

All these objects had absorption and fluorescence contrast in the NIR range sufficient for their detection (Figure 6A–E). The clearance rate after intravenous injection varied from 23 days for highly stable liposomes and 6 days for ICG labeled RBCs to just a few hours for MTLn3-iRFP cells. Circulation kinetics studies by the integrated PAFFC revealed the re-appearance of MTLn3-iRFP cells in circulation, obviously due to the establishment distant metastases [13] and an increased number of clustered liposomes on 15th day of monitoring.

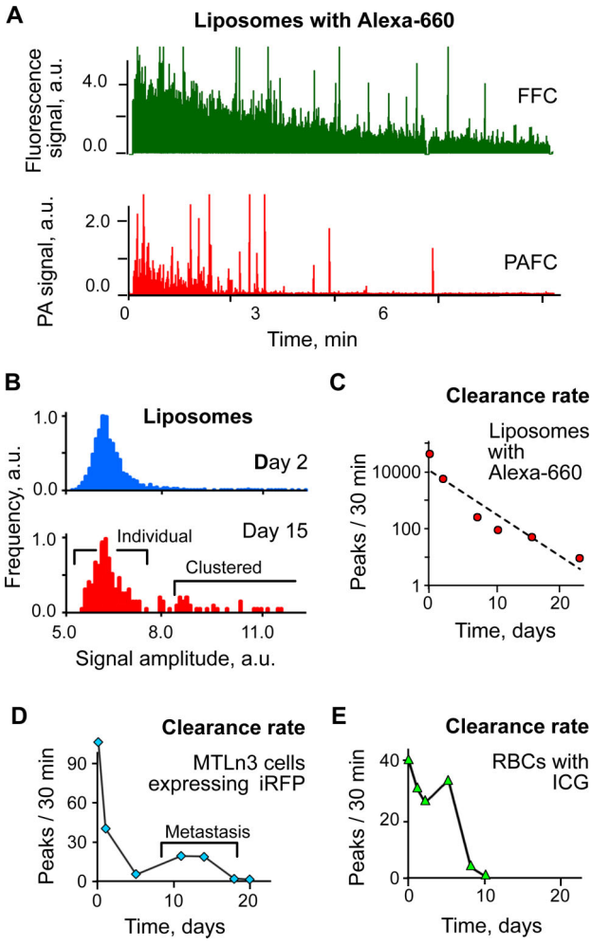

Figure 6 *In vivo* detection of circulating objects labeled by NIR fluorophores: Alexa-660, ICG, and iRFP. (**A**) PA and fluorescence detection of liposomes loaded with Alexa-660. (**B**) Histogram analysis of signal amplitudes from liposomes on 2nd and 15th days after injection (total of 12500 and 192 peaks, respectively). (**C**) Long-term circulation kinetics for liposomes, cancer cells and RBCs obtained by PAFFC. Laser parameters: wavelength 671 nm, energy fluence 200 mJ/cm^2.

3.4 Multimodal photoacoustic and fluorescence flow cytometry using negative and positive contrast

Recently we introduced a negative contrast PAFC [19] in which low absorbing circulating objects (e.g., white platelet-rich clots) produced negative peaks in the blood absorption background (Figure 1C). The potential of negative contrast to identify strongly absorbing RBCs in the presence of a strong fluorescence background was also demonstrated [19]. Integration of positive and negative contrasts in multimodal PAFFC may significantly enhance its synergistic capability for label-free detection of cells using absorption and fluorescence properties (Figure 7).

At the first stage, the integrated PAFFC was used to monitor fluorescent cells having low pigmentation. Relatively transparent melanoma C8161-GFP cells with low melanin-associated pigmentation [22, 24] simultaneously provided positive fluorescence and negative PA signals for both single cells and cell aggregates (Figure 8A). These data demonstrated that negative contrast PA cytometry is capable of detecting single, low absorbing cells with sizes as small as 20 μm identified in 30–50 μm blood vessels. We believe that further enhancement in the spatial resolution of PAFC through improved optical and acoustic focusing may allow counting of various non-pigmented CTCs and WBCs in blood flow.

On the second stage, we estimated the diagnostic value of fluorescence imaging cytometry using negative contrast of RBCs. In this case, the fluorescence background was created by autofluorescence of plasma and tissues (Figure 7A). Negative contrast of RBCs in plasma (Figure 7B) allowed label-free fluorescence imaging cytometry of single RBCs in tiny ear capillaries (Figure 8B) and of clots in mouse mesentery vein (Figure 8C). Mesentery imaging also re-

Journal of
BIOPHOTONICS

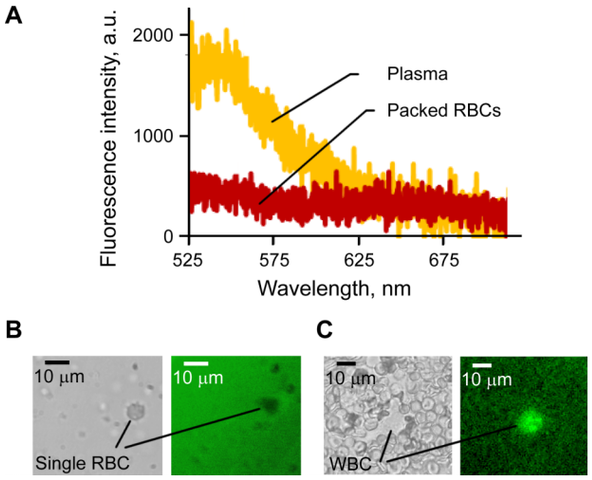

Figure 7 Fluorescence of blood components. (**A**) Fluorescence spectra of purified blood plasma and RBCs. (**B**, **C**) Transmission and fluorescence images (left and right, respectively) of a single RBC in blood plasma (**B**) and of a single WBC among RBCs (**C**).

vealed negative fluorescence contrast of adypocytes that may be used for their detection and identification. Plasma fluorescence may be enhanced by injecting fluorescent dye. *In vivo* fluorescence image flow cytometry in a 40 μm ear vein after injection of FITC-Dextran revealed individual and aggregated RBCs (Figure 8B) having negative fluorescence contrast.

Finally, we performed *in vivo* flow cytometry to detect circulating clots using intrinsic fluorescence contrast of blood plasma components (Figure 7). A photothrombotic clot was created in the mouse vein by exposing it to 488 nm laser at an intensity of 10^3 W/cm^2 for 60 s. The adhered clot (Figure 8E) had a negative contrast in transmission and positive contrast in fluorescence modes, respectively. Flow cytometry data demonstrated a transient increase in fluorescence intensity (Figure 8F, top) that coincided with the passage of the clot, which was observed by transmission microscopy (data is not presented here). Thus, a clot, having few RBCs and many platelets (Figure 7C) significantly increased fluorescence intensity. On the other hand, aggregated RBCs strongly reduced the autofluorescence background as compared to non-aggregated RBCs and, thus, produced a transient negative peak (Figure 8F, bottom). We have observed such negative peaks after inflicting laser damage to the mice's tail vein. No negative peaks were observed in these mice before the damage. Still, this is preliminary data and requires an additional verification to be addressed in future papers.

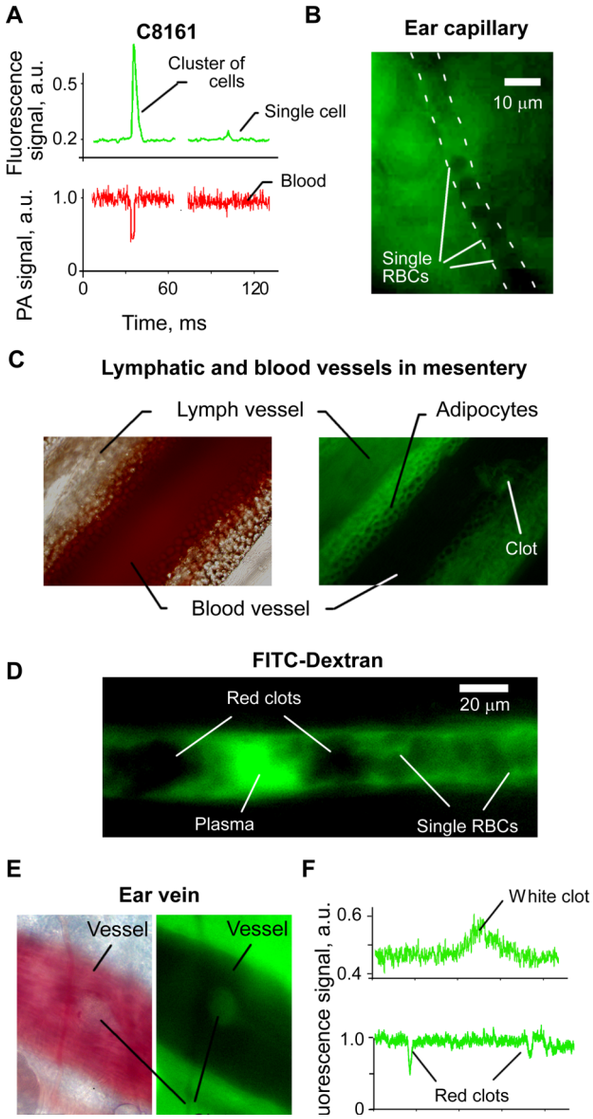

Figure 8 Positive and negative contrasts in fluorescence cytometry. **A**, Typical negative PA and positive fluorescence contrast signals from circulating C8161-GFP cells in 40 μm artery. PAFC and FFC parameters: 820 nm, 50 mJ/cm^2 and 488 nm, 80 W/cm^2, respectively. (**B**) Fluorescence imaging cytometry of single RBCs (negative contrast) in mouse ear capillary. (**C**) Transmission (left) and fluorescence (right) imaging of blood and lymph vessels in mouse mesentery. Clots in the blood vessel appears brighter than the blood. (**D**) Fluorescence imaging cytometry of single and aggregated RBCs in 40 μm mouse ear vein. Background plasma fluorescence was enhanced by FITC-Dextran. (**E**) *In vivo* imaging of an adhered white clot. Negative contrast in transmission (left) and positive in fluorescence (right) imaging modes. (**F**) *In vivo* FFC monitoring of the clots in circulation. White photothrombotic clot had positive contrast (top), while negative fluorescence contrast was associated with red clots (bottom). Laser wavelength, intensity: 488 nm, 80 W/cm^2.

4. Discussion

We demonstrated that integrated PA-fluorescence cytometry is capable of simultaneously monitoring various agents having dominant PA, fluorescent or both contrasts *in vivo* in blood flow. Combination of fluorescence and PA tags eliminates spectral overlapping between them and makes it possible for these two tags to co-exist in the same spectral region.

Potential applications of integrated techniques include characterization and enumeration of circulating blood and tumor cells, viruses, NPs and drug delivery vehicles (liposomes) using fluorescent and PA tags. Fluorescent detection of genetically encoded fluorescent proteins and PA detection of light absorbing NPs reveals the fate of nanomaterials in the blood system, including the interaction of NPs with the cells of the immune system or with tumor cells in blood flow, study of infections and etc. For example, we have previously demonstrated WBC labeling by gold nanorods conjugated to anti-CD45-antibody [26]. On the other hand, the fluorescence flow cytometry has also been used for T-cells studies [5, 27, 28]; thus, the integrated cytometry method would benefit from the increased number of possible labels and would allow direct studies of immune system responses and of T-cells, in particular. Currently, various nanomaterials are considered for the use in humans, such as gold-based NPs [29]. PAFFC may reveal new aspects of their interaction with blood, and T-cells, and may guide therapy of circulating abnormal cells (e.g., bacteria or tumor cells) [13].

The application of the integrated cytometer toward studies of cells interaction with NPs was demonstrated *in vivo* for C8161-GFP melanoma CTCs and 50 nm magnetic NPs conjugated with antibodies specific to melanoma MCSP receptors. Fluorescent and PA peaks distinguished CTCs expressing MCSP from the melanoma cells not-expressing it and minimized the rate of false positive signals from unbound single and aggregated NPs. Total CTCs and MCSP-CTCs counts were obtained *in vivo* without the need of bleeding mice for *ex vivo* blood analysis. This approach can be applied toward a wide range of cancer types using multicolor cytometry and multi-marker labeling [30]. Common receptors like EpCAM or folate may be used to target CTC in the blood or lymph flow [4, 5], and a second label, such as the anti-MCSP-beads reported here, may be used to count cells expressing a particular protein. In this case, the integrated PAFFC would eliminate cross-talk between the signals, thus further increasing detection specificity and accuracy.

Multimodal techniques provide a method to compare the detection of the individual objects in different modes and performing cross-verification of the data (i.e. PA vs. fluorescence). This has high importance *in vivo*, where few independent controls or standard calibration procedures may be implemented. Fluorescent or light absorbing microbeads widely used *in vitro* for system calibration may be affected *in vivo* by biocompatibility issues or cause an acute immune system response. With fluorescence monitoring of B16F10 melanoma cells labeled with FITC, we demonstrated a direct verification of label-free PA detection. This verification confirmed our previous relevant data [13, 24]. The integrated system implemented all the calibration procedures in a single experiment, and avoided time-consuming *in vitro* verification tests.

For the first time, we have presented the results of simultaneous PA and fluorescence detection in flow cytometry mode using only nanosecond pulsed laser sources. Specifically, 671 nm pulsed laser provided multimodal detection for ICG (approved for the use in humans) and near-infrared iRFP protein. The bacteriophytochrome-derived iRFP protein provides genetically encoded detection in NIR tissue transparency window [23]. For superficial microvessels the sensitivity of PA detection of NIR fluorophores was lower compared to that of fluorescence detection. However, the sensitivity of the PA technique is much more promising in deeper vessels that are not reachable using fluorescence method.

We also demonstrated the supplementary nature of PA and fluorescence contrasts of blood which may dramatically improve label-free identification of clots and even of individual cells by PAFFC. Red and white clots [19] may be enumerated in blood using their positive and negative PA contrasts, respectively. However, in fluorescence mode, the same objects would have negative and positive contrasts (Figures 7 and 8), respectively. In this case, autofluorescence background, as a problem in conventional positive contrast FFC, becomes an advantage in the integrated method, potentially providing a dramatic increase in detection accuracy and in the elimination of false-positive signals.

From our point of view, further development of an integrated *in vivo* flow cytometer should further increase the multicolor capability in both fluorescent and PA modes. In this case, fluorescence cytometry may be oriented on multicolor detection in 500–650 nm wavelength range suitable for the majority of existing fluorophores. PA detection [13] would have the highest sensitivity in the NIR tissue transparency window (650–1100 nm) and may rely on light absorbing NPs like gold nanorods exhibiting widely tunable absorbances [14].

We determined that PAFFC has the highest sensitivity in noninvasive monitoring of superficial 40–80 μm mouse ear arteries and veins. However, PA detection alone was shown to operate even in 1 mm thick veins [13]. The particularities of fluorescence detection limit the use of larger blood vessels. Thus,

Journal of
BIOPHOTONICS

PA and fluorescent cytometry methods may provide both detection of rare events (PA mode only) and multicolor-multimode characterization of the cells in superficial blood vessels in the integrated mode for research purposes.

5. Conclusion

Our data have shown that the PA and fluorescence detection beneficially complement each other and have a broad spectrum of potential applications including detection of CTCs, bacteria, viruses, and capsulated drugs with various fluorescent and absorption properties. Pulsed excitation decreases the exposure of tissues to laser light by generating two independent signals and provides an opportunity to double or even triple a number of the labeling tags in the same spectral range.

Acknowledgements This work was supported by the NIH grants EB000873, CA131164, EB009230, CA139373, GM073913, CA164468, CA113796, CA138231 and CA093683 and by the D Department of Defense grants W88XWH-10-2-0130, W81XWH-10-BCRP-CA and W81XWH-11-1-0129. We thank Dr. J.-H. Ye for the help with cell cultures.

Author biographies Please see Supporting Information online.

References

[1] H. M. Shapiro, Practical flow cytometry (Wiley-Liss, New York, 2003), p. 681.
[2] E. Schulze, C. Siewert, M. Herber, J. Schmitz, M. Assenmacher, and S. Miltenyi, Cytometry **46**, 193 (2001).
[3] C. Siewert, M. Herber, O. Fodstad, S. Miltenyi, M. Assenmacher, and J. Schmitz, Recent Results Cancer Res. **158**, 51 (2001).
[4] V. V. Tuchin, A. Tárnok, and V. P. Zharov, Cytometry A **79**, 737 (2011).
[5] C. M. Pitsillides, J. M. Runnels, J. A. Spencer, L. Zhi, M. X. Wu, and C. P. Lin, Cytometry A **79**, 758 (2011).
[6] L. Zhang, C. Alt, P. Li, R. M. White, L. I. Zon, X. Wei, and C. P. Lin, Cytometry A, **81**, 176 (2012).
[7] E. Zettergren, D. Vickers, J. Runnels, S. K. Murthy, C. P. Lin, and M. Niedre, J. Biomed. Opt. **17**, 037001 (2012).
[8] V. Zharov, E. Galanzha, and V. Tuchin, Proc. SPIE **5320**, 185 (2004).
[9] J. Novak, I. Georgakoudi, X. Wei, A. Prossin, and C. P. Lin, Opt. Lett. **29**, 77 (2004).
[10] V. P. Zharov, E. I. Galanzha, E. V. Shashkov, N. G. Khlebtsov, and V. V. Tuchin, Opt. Lett. **31**, 3623 (2006).
[11] A. S. Biris, E. I. Galanzha, Z. R. Li, M. Mahmood, Y. Xu, and V. P. Zharov, J. Biomed. Opt. **14**, 3119145 (2009).
[12] E. R. Tkaczyk and A. H. Tkaczyk, Cytometry A **79**, 775 (2011).
[13] E. I. Galanzha, E. V. Shashkov, P. M. Spring, J. Y. Suen, and V. P. Zharov, Cancer Res. **69**, 7926 (2009).
[14] V. P. Zharov, Nature Photon. **5**, 110 (2011).
[15] V. P. Zharov, E. I. Galanzha, and V. V. Tuchin, J. Cell Biochem. **97**, 916 (2006).
[16] E. I. Galanzha, V. V. Tuchin, and V. P. Zharov, World J. Gastroenterol. **13**, 192 (2007).
[17] Y. Wang, K. Maslov, C. Kim, S. Hu, and L. H. V. Wang, IEEE Trans. Bio-Med. Eng. **57**, 2576 (2010).
[18] D. Razansky and V. Ntziachristos, Med. Phys. **34**, 4293 (2007).
[19] E. I. Galanzha, M. Sarimollaoglu, D. A. Nedosekin, S. G. Keyrouz, J. L. Mehta, and V. P. Zharov, Cytometry A **79**, 814 (2011).
[20] D. A. Nedosekin, E. I. Galanzha, S. Ayyadevara, R. J. S. Reis, and V. P. Zharov, Biophys. J. **102**, 672 (2012).
[21] D. A. Nedosekin, M. V. Khodakovskaya, A. S. Biris, D. Wang, Y. Xu, H. Villagarcia, E. I. Galanzha, and V. P. Zharov, Cytometry A **79**, 855 (2011).
[22] J. Ma, J. Y. Lin, A. Alloo, B. J. Wilson, T. Schatton, Q. A. Zhan, G. F. Murphy, A. M. Waaga-Gasser, M. Gasser, F. S. Hodi et al., Biochem. Bioph. Res. Co. **402**, 711 (2010).
[23] G. S. Filonov, K. D. Piatkevich, L. M. Ting, J. H. Zhang, K. Kim, and V. V. Verkhusha, Nat. Biotechnol. **29**, 757 (2011).
[24] D. A. Nedosekin, M. Sarimollaoglu, J.-H. Ye, E. I. Galanzha, and V. P. Zharov, Cytometry A **79**, 825 (2011).
[25] U. Resch-Genger, M. Grabolle, S. Cavaliere-Jaricot, R. Nitschke, and T. Nann, Nat. Methods **5**, 763 (2008).
[26] M. Sarimollaoglu, D. A. Nedosekin, Y. Simanovsky, E. I. Galanzha, and V. P. Zharov, Opt. Lett. **36**, 4086 (2011).
[27] Z. Fan, J. A. Spencer, Y. Lu, C. M. Pitsillides, G. Singh, P. Kim, S. H. Yun, V. Toxavidis, T. B. Strom, C. P. Lin and others, Nat. Med. **16**, 718 (2010).
[28] C. Pitsillides, P. Zamiri, J. Novak, and C. P. Lin, Invest. Ophthalmol. Vis. Sci. **46**, (2005).
[29] A. S. Thakor, J. Jokerst, C. Zavaleta, T. F. Massoud, and S. S. Gambhir, Nano Lett. **11**, 4029 (2011).
[30] E. I. Galanzha, E. V. Shashkov, T. Kelly, J. W. Kim, L. L. Yang, and V. P. Zharov, Nat. Nanotechnol. **4**, 855 (2009).

